

Simulation of Self Tuning Shape Memory Alloy Based PZT Energy Harvester

M. G. Vasundhara¹, G. K. Kalavathi^{2*}, E. L. Pradeesh³, K. K. Yogesha⁴, H. R. Prakash⁵, B. Muralidhara⁶ and B. Hulugappa⁴

¹Department of Mechanical Engineering, Malnad College of Engineering, Hassan – 573202, Karnataka, India; mgv@mcehassan.ac.in

²Department of Mathematics, Malnad College of Engineering, Hassan – 573202, Karnataka, India; gkk@mcehassan.ac.in

³Department of Mechatronics, Bannari Amman Institute of Technology, Sathyamangalam – 638401, Tamil Nadu, India; pradeesh.dmt@gmail.com

⁴Department of Mechanical Engineering, National Institute of Engineering, Mysuru – 570008, Karnataka, India; yogeshakk@nie.ac, muraligeck@gmail.com

⁵Department of Mechanical Engineering, BMS College of Engineering, Bangalore – 560019, Karnataka, India; prakashhr73@gmail.com

⁶Department of Mechanical Engineering, Government Engineering College, Mosale Hosahalli, Hassan – 573212, Karnataka, India

Abstract

Shape Memory Alloy (SMA) is tuned to match the frequency of excitation with the resonance frequency. Simulation is carried out numerically using COMSOL 5.3 software. This model consists of cantilevered beam without tip mass, PZT layer, Aluminium beam and SMA layer. Lead Zirconium titanate (PZT – 5A) is used as PZT layer for the conversion of energy. Harvesters power frequency response for different frequency ranges are carried out. The maximum output is obtained in excitation frequency with SMA and the results were compared without SMA material. The numerical simulation of the Frequency Response Functions (FRF) was compared with the analytical frequency response functions of the harvester. The maximum difference between the numerical and analytical results is 9.77 % in FRF's and 1.85 % in resonance frequency. Materials used are Lead Zirconium titanate (PZT – 5A), SMA material and Aluminium beam which reaches the scopes of journal.

Keywords: Energy Harvester, Numerical Simulation, PZT, Shape Memory Alloy

1.0 Introduction

Energy harvester captures the ambient frequency from the different sources of the environment like sunlight, pressure, mechanical vibration, wind and converts it to electrical power. This harvested energy is stored in circuits with capacitors as well as batteries and used to

power electronic and electrical devices such as wireless sensors, micropumps, etc. Hence this portable electronic equipment becomes self-powered. For many years' energy harvesting is processed using Piezoelectric (PZT) material which converts mechanical energy into a voltage output. Researchers studied the numerical model of energy harvester using finite element method. Mohsen Safaei

*Author for correspondence

reviewed the summarization of various developments on energy harvesting using PZT¹. Energy harvesting using a dynamic magnifier is studied numerically using the Hamilton principle². Kim *et al.*³ developed a numerical model of Shape memory alloy plate reflecting the tension/compression asymmetry of axial stress due to pure bending and ABAQUS was used for efficient computation and verified experimentally later. The tunable shape memory alloy based harvesting energy with piezoelectric material by changing SMA's martensite volume fraction is studied⁴⁻⁶. Numerical simulation as well as analytically studied energy harvesting using MEMS devices in nonlinear regim⁷ Belkourchia *et al.*⁸ studied the simulation of energy harvesting for the FSI model from ocean waves and beams using PZT material. Mekhalifa⁹ optimized thermal energy harvesting by PZT using shape memory alloy. Many researchers worked on energy harvesting using PZT material¹⁰⁻¹⁷. The proposed model consists of a cantilevered beam without tip mass composed of PZT, substructure and SMA material. To alter the natural frequency of composite cantilever beam SMA material is used. The maximum output is obtained

in excitation frequency with SMA and the results were compared without SMA material.

2.0 Simulation using COMSOL

Figure 1 shows the SMA based tunable PZT energy harvester with base excitation without tipmass. This is modelled using the finite element method in COMSOL Multiphysics 5.3 software and used to know the response function of frequency like power FRF.

Figure 2 shows the rectangular-shaped cantilevered energy harvester with three dimensional geometry. This beam consists of a PZT layer at the top, the Aluminium beam is used as substructure in the middle and SMA layer is attached to the bottom. For energy conversion, lead Zirconium titanate (PZT – 5A) is used. SMA is used to tune the harvester resonant frequency. Table 1 shows the material properties and harvester dimensions.

A tunable SMA based energy harvester is fixed at one end by applying fixed constraints on the vertical face to all three layers. On the other end, all three layers are left free to vibrate in the vertical direction. Input force per unit

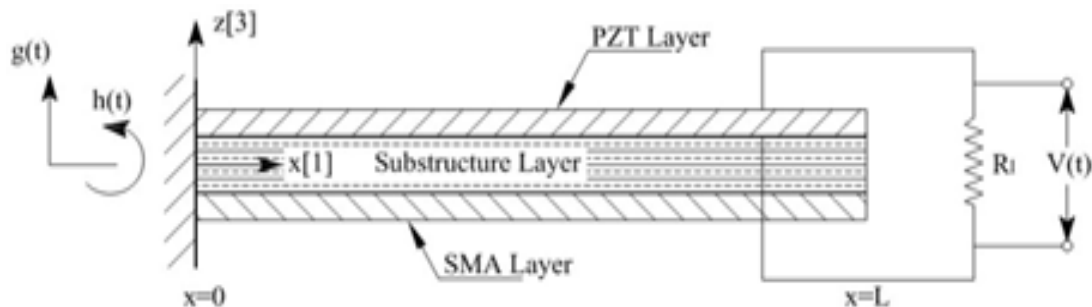


Figure 1. SMA based frequency tunable piezoelectric energy harvester.

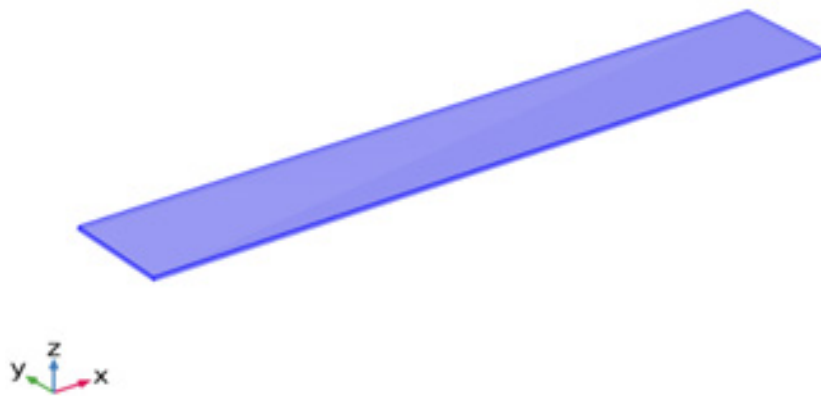


Figure 2. Geometry of the SMA based tunable energy harvester.

Table 1. Properties and geometry of the tunable SMA based energy harvester

| | |
|------------------------------------|-------|
| Length of beam, | 32 |
| Width of the beam, | 5 |
| Thickness of PZT, | 0.15 |
| Thickness of substructure, | 0.05 |
| Mass moment of inertia at the tip, | |
| Youngs modulus of PZT, | 61 |
| Youngs modulus of substructure, | 100 |
| Youngs modulus of austenite | 73.3 |
| Youngs modulus of martensite | 30 |
| Maximum residual strain | 10 |
| Martensite start stress, | 371 |
| Martensite final stress, | 613.3 |
| Mass density of PZT, | 7750 |
| Mass density of substructure, | 2700 |
| Mass density of SMA, | 6500 |
| Piezoelectric constant, | -10.4 |
| Permittivity constant, | 13.3 |

volume is applied to the cantilevered beam as an energy source. In order to pole, the upper face of the piezoelectric layer is connected to d31 mode with floating potential and grounding is applied in the bottom face PZT layer. The

remaining faces of the PZT layer are charged with zero constraints. External load resistance is applied through the electrostatic circuit.

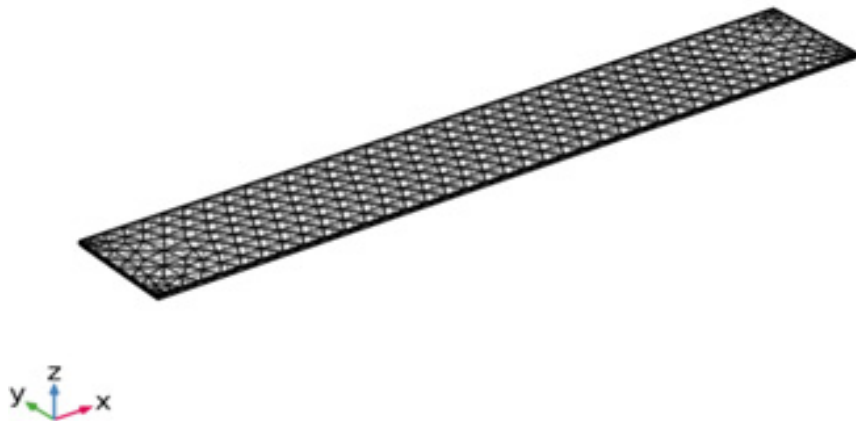
2.1 Finite Element Discretization

To obtain more accurate results for frequency and higher order mode shapes a very fine mesh is used in COMSOL. The density of mesh is changed in six different shapes with different sizes of elements from extreme coarse (8057 elements) to fine coarse (234462 elements) to check the simulation effect on computation time. Using physics controlled sequence, the tetrahedral elements with coarse mesh 37298 elements are used to minimise the computation time. Figure 3 shows the meshed model with 5007 domain elements in the global model, 408 elements in edge, 2816 elements in the boundary and 29607 elements in degree freedom. Fixed state condition is considered in the simulation of this model. Global response of the SMA based tunable energy harvester subjected to harmonic excitation is solved using a MUMPS solver.

2.2 Mathematical Model of the Tunable Energy Harvester without Tip mass

The non-linear partial differential equation for SMA based PZT energy harvester without tip mass is given by

$$-\frac{\partial^2 N(x, t)}{\partial x^2} + d_s l \frac{\partial^5 U_{rel}(x, t)}{\partial x^4 \partial t} + d_a \frac{\partial U_{rel}(x, t)}{\partial t} + m \frac{\partial^2 U_{rel}(x, t)}{\partial t^2} = -m \frac{\partial^2 U_b(x, t)}{\partial t^2}. \quad (1)$$

**Figure 3.** Meshed model of the SMA based tunable energy harvester.

where, $N(x,t)$ is internal bending moment, $U_{rel}(x,t)$ is the displacement of the beam in transverse direction, $d_s I$ denotes the composite beam damping constant, d_a is

constant of viscous air damping, m is mass per unit length of beam, L is the length of beam, and $U_b(x,t)$ is the base excitation.

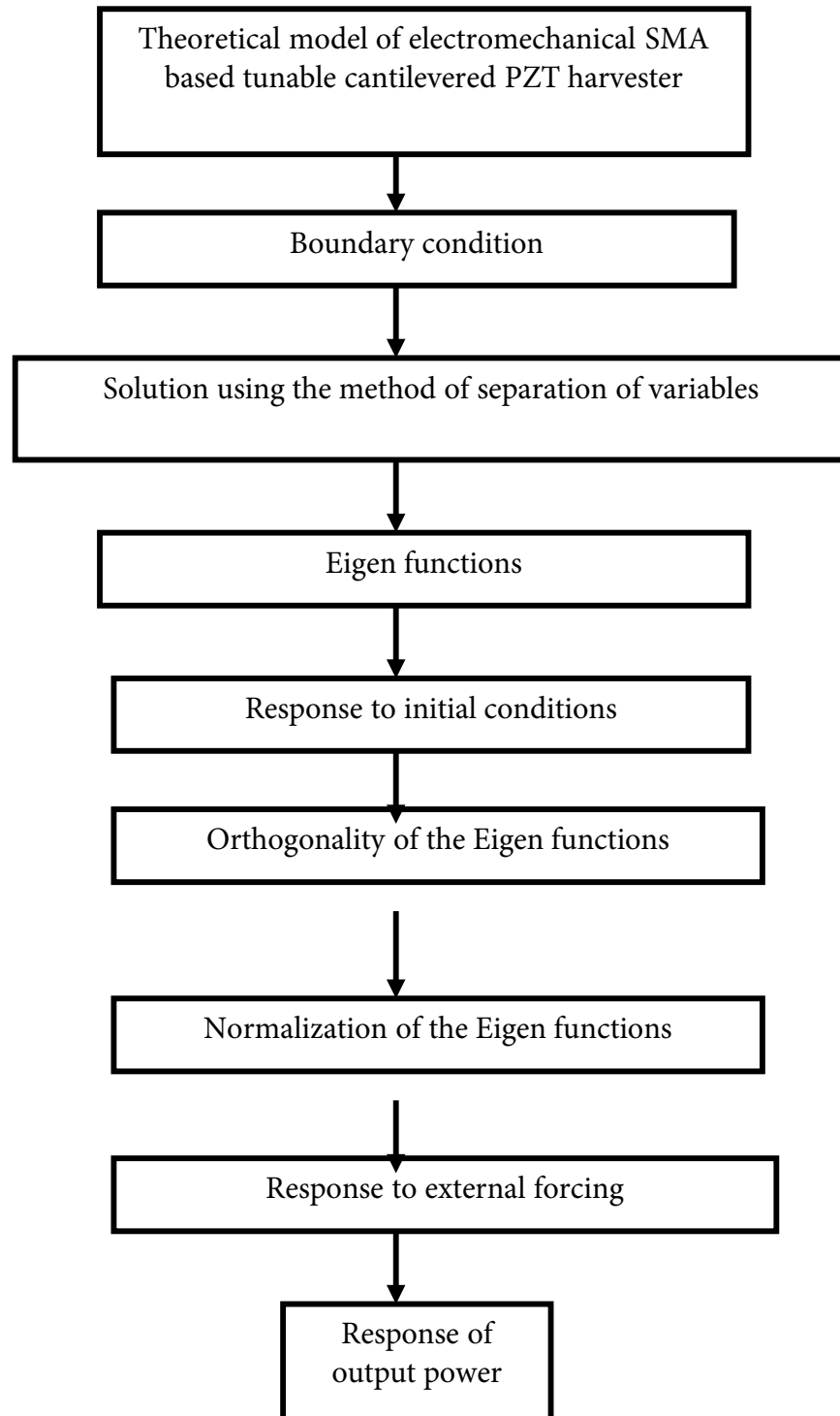


Figure 4. Flowchart for modal analysis of the harvester.

Flowchart as shown in Figure 4 shows the algorithm for solving the problem. The expression for the power frequency response function is given in Equation (2)⁴.

$$\frac{p(t)}{(-\omega^2 e^{j\omega t})^2} = \frac{1}{R_l} \left(\frac{\sum_{k=1}^{\infty} \frac{-j\omega\theta_k M_k}{\phi_k^2 - \omega^2 + j2\xi_k\phi_k\omega}}{\frac{1}{R_l} + j\omega C_p + \sum_{k=1}^{\infty} \frac{j\omega\theta_k^2}{\phi_k^2 - \omega^2 + j2\xi_k\phi_k\omega}} \right)^2 \quad (2)$$

Here, M_k amplitude of mechanical forcing function, ξ_k damping ratio, ω frequency of the excitation, R_l resistive load, ϕ_k undamped natural frequency, θ_k modal coupling, C_p equivalent capacitance, t time constant, k denotes the number of modes, and $j = \sqrt{-1}$.

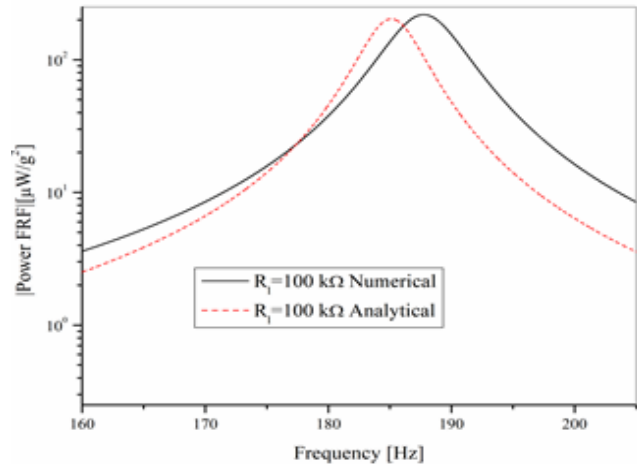


Figure 7. Power FRF for the first mode of vibration $\zeta_s=1$.

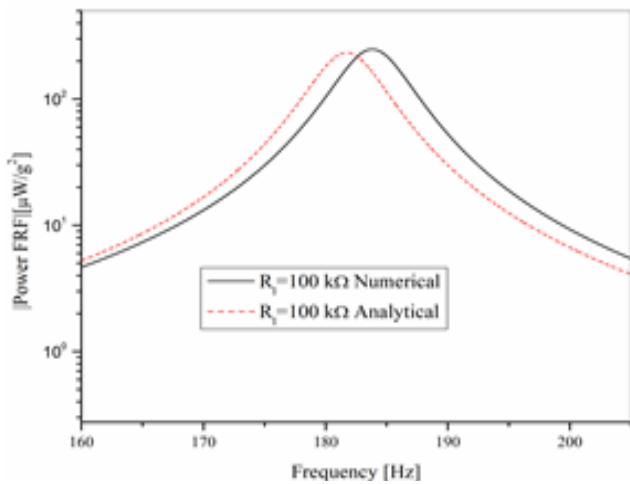


Figure 5. Power FRF for the first mode of vibration $\zeta_s=0$.

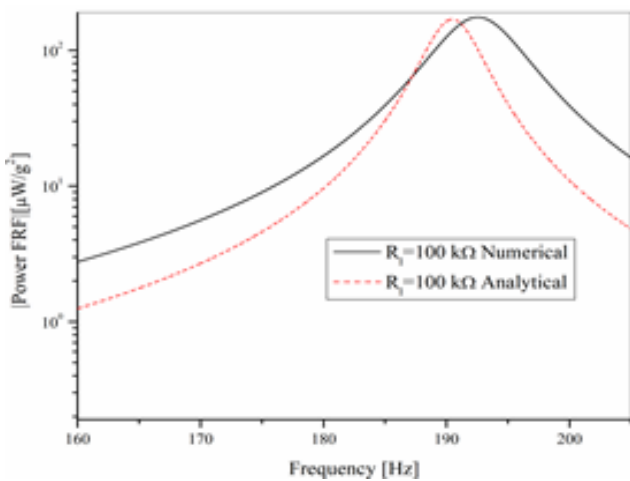
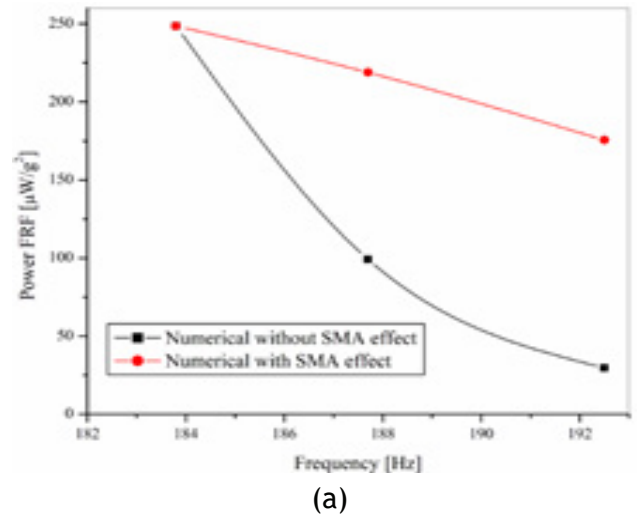
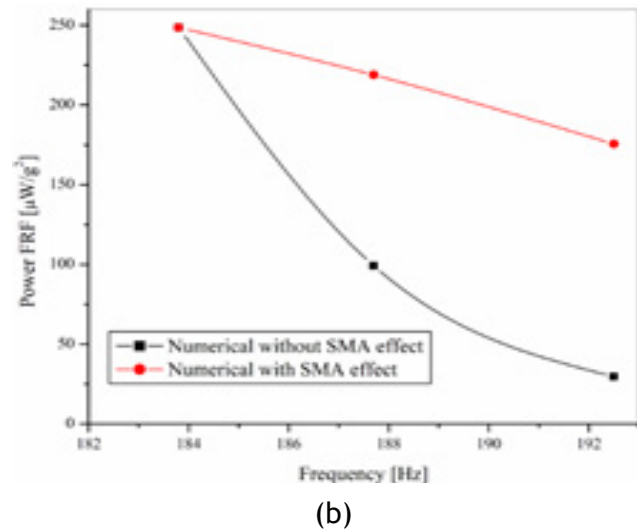


Figure 6. Power FRF for the first mode of vibration $\zeta_s=0.5$.



(a)



(b)

Figure 8. Power FRF with/without SMA effect at $R_l=100$ kΩ (a) Analytical (b) Numerical.

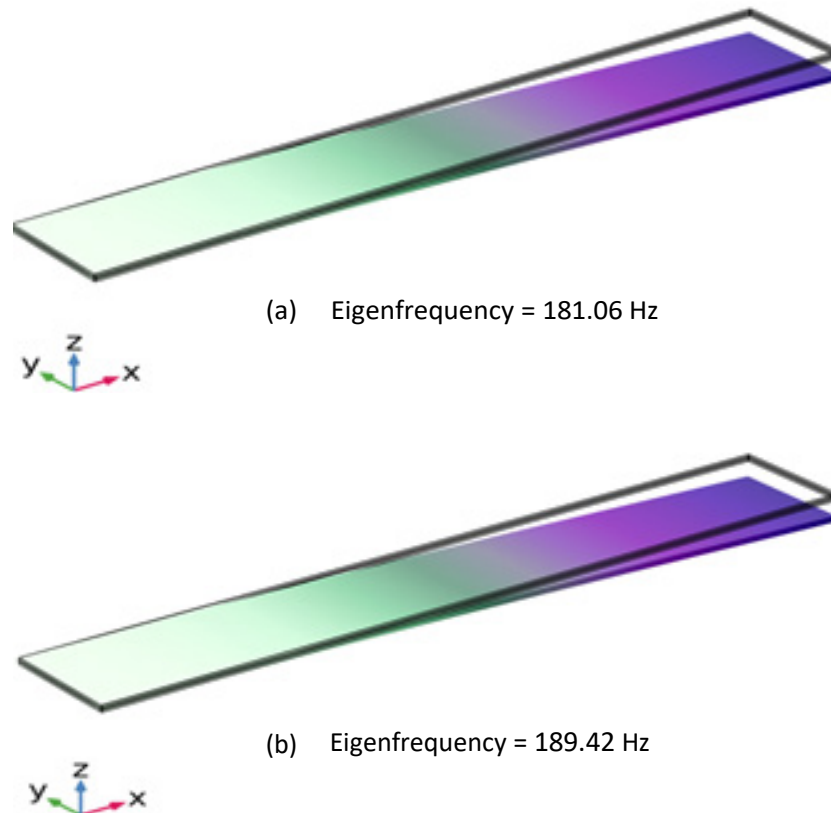


Figure 9. Eigen Frequencies (a) 181.06 Hz (b) 189.42 Hz.

3.0 Simulation and Discussion

Self-tuning electromechanical SMA based PZT energy harvester is simulated to study the frequency response function power and eigen frequency in the frequency domain. For the first mode of vibration, the tunable SMA based energy harvester is simulated to match resonant/excitation frequency with natural frequency for power FRF. Numerical results are compared with

the analytical results for different types of martensite volume fractions $\zeta_s=0, 0.5$ and $\zeta_s=1$. A graph of power FRF versus frequency for various load resistance R_l and different martensite volume fraction ζ_s are drawn for the first mode of vibration shown in Figures 5–7. It is observed that maximum power output is obtained at $R_l=100 \text{ k}\Omega$ for $\zeta_s=0$ and $\zeta_s=1$. The power FRF outputs produced from piezoelectric for different volume fraction at resonant frequency are tabulated in Tables 2 and 3 for

Table 2. Comparison of short and open circuit resonance frequencies for numerical and analytical model

| Model | Analytical | | | | Numerical | | | |
|---------------------------------|-------------|-------------|-------|------------|-------------|-------------|-------|------------|
| | $\zeta_s=0$ | $\zeta_s=1$ | shift | Tuning (%) | $\zeta_s=0$ | $\zeta_s=1$ | shift | Tuning (%) |
| f_k^{sc} (Hz) (short circuit) | 179.5 | 189.3 | 9.8 | 5.5 | 181.3 | 189.7 | 8.4 | 4.6 |
| f_k^{oc} (Hz) (open circuit) | 183.0 | 191.1 | 8.1 | 4.4 | 184.7 | 193.5 | 8.8 | 4.8 |

Table 3. Comparison of numerical and analytical power FRF and corresponding resonance

| Optimum load (Ω) | Analytical frequency (Hz) | Numerical frequency (Hz) | Deviation (%) | Analytical power ($\mu\text{W}/\text{g}^2$) | Numerical power in ($\mu\text{W}/\text{g}^2$) | Deviation (%) |
|---------------------------|---------------------------|--------------------------|---------------|---|---|---------------|
| $\zeta_s=0$ | | | | | | |
| 100 k | 181.7 | 183.8 | 1.16 | 234.01 | 248.59 | 6.23 |
| $\zeta_s=0.5$ | | | | | | |
| 100 k | 185.1 | 187.7 | 1.40 | 203.65 | 218.81 | 7.45 |
| $\zeta_s=1$ | | | | | | |
| 100 k | 190.5 | 192.5 | 1.05 | 169.56 | 175.53 | 3.52 |

Table 4. Comparison of numerical and analytical natural frequencies for first mode without electric circuit

| Volume fraction | Analytical frequency (Hz) | Numerical frequency (Hz) | Deviation (%) |
|-----------------|---------------------------|--------------------------|---------------|
| $\zeta_s=0$ | 179.5 | 181.06 | 0.87 |
| $\zeta_s=1$ | 189.3 | 189.42 | 0.06 |

both analytical and numerical results. The maximum difference between the numerical and analytical results is 7.45% in power FRF and 1.40% in resonance frequency.

Power FRF of energy harvester with SMA effect is higher compared to without SMA in both numerical and analytical methods is shown in Figure 8. The model is simulated for eigen frequency by using finite element analysis without considering the electric circuit and compared with the analytical natural frequency, which is tabulated in Table 4. The first mode shape and corresponding eigen frequency are shown in Figure 9 for

the different martensite volume fraction $\zeta_s=0$ and $\zeta_s=1$. The physical models are simulated as accurately as possible to align as closely with analytical results. The maximum deviation between the simulation and analytical results is 0.87% only.

4.0 Validation

The natural frequencies of PZT harvester's numerical results closely resembled the analytical results and also

Table 5. Comparison of the numerical, analytical and experimental natural frequencies

| Proposed model | | | Validated with ¹⁸ | | |
|--------------------------|---------------------------|---------------|------------------------------|-----------------------------|---------------|
| Numerical frequency (Hz) | Analytical frequency (Hz) | Deviation (%) | Numerical frequency (Hz) | Experimental frequency (Hz) | Deviation (%) |
| 179.5 | 181.06 | 0.87 | 94.5 | 93.7 | 0.85 |

the deviation of this result is in good agreement with the result of ¹⁸(Table 5).

5.0 Conclusion

Numerical study on cantilevered energy harvester consists of Piezoelectric (PZT) layer, substructure layer and shape memory alloy is studied. The numerical simulation of the frequency response functions was compared with the analytical frequency response functions of the harvester. The maximum differences between the numerical and analytical results are 9.77% in FRF's and 1.85% in resonance frequency. The numerical results of FRF of the harvester's power indicated a good agreement with the results of the analytical results of FRF's.

6.0 Acknowledgements

This work was supported by Department of Information Technology, BioTechnology and Science and Technology, Government of Karnataka, India (Grant number: KSTePS/VGST-RGS/F/GRD No.692/2017-18).

7.0 References

1. Safaei M, Sodano HA, Anton SR. A review of energy harvesting using piezoelectric materials: State-of-the-art a decade later (2008-2018). *Smart Mater Struct.* 2019 Oct; 28(11). <https://doi.org/10.1088/1361-665X/ab36e4>
2. Tang L, Wang J. Size effect of tip mass on performance of cantilevered piezoelectric energy harvester with a dynamic magnifier. *Acta Mech.* 2017 Nov; 228(11):3997-4015. <https://doi.org/10.1007/s00707-017-1910-8>
3. Kim Y-J, Lee C-H, Kim J-H, Lim JH. Numerical modeling of shape memory alloy plates considering tension/compression asymmetry and its verification under pure bending. *Int J Solids Struct.* 2018 Apr; 136-137:77-88. <https://doi.org/10.1016/j.ijsolstr.2017.12.004>
4. Senthilkumar M, Vasundhara MG, Kalavathi GK. Electromechanical analytical model of shape memory alloy based tunable cantilevered piezoelectric energy harvester. *Int J Mech Mater Des.* 2018 Aug; 15:1-17.
5. Vasundhara MG, Senthilkumar M, Kalavathi GK. A distributed parametric model of shape memory alloy-based resonant frequency tunable cantilevered PZT energy harvester with tip mass. *ISSS J Micro Smart Syst.* 2019 Apr; 8:1-12. <https://doi.org/10.1007/s41683-019-00034-0>
6. Vasundhara MG, Senthilkumar M, Kalavathi GK. A distributed parametric model of Brinson shape memory alloy based resonant frequency tunable cantilevered PZT energy harvester. *Int J Mech Mater Des.* 2018 Nov; 15:55-68.
7. Pasharavesh A, Ahmadian MT. Analytical and numerical simulations of energy harvesting using MEMS devices operating in nonlinear regime. *Eur Phys J B.* 2018 Oct; 91(10). Available from: <https://doi.org/10.1140/epjb/e2018-80609-8>
8. Belkourchia Y, Bakhti H, Azrar L. Numerical simulation of FSI model for energy harvesting from ocean waves and beams with piezoelectric material. In: *Proceedings of 2018 6th International Renewable and Sustainable Energy Conference, IRSEC 2018.* Institute of Electrical and Electronics Engineers Inc.; 2018. <https://doi.org/10.1109/IRSEC.2018.8702943>
9. Mekhafia ML. Optimization of thermal energy harvesting by PZT using shape memory alloy. *Energy Harvest Syst.* 2021 Mar; 7(1). <https://doi.org/10.1515/ehs-2020-0003>
10. Bakhtiari-Shahri M, Moeenfarid H. Energy harvesting from unimorph piezoelectric circular plates under random acoustic and base acceleration excitations. *Mech Syst Signal Process.* 2019 Sep; 130:502-23. <https://doi.org/10.1016/j.ymssp.2019.05.017>
11. Prauzek M, Konecny J, Vitasek M, Bajgar V, Musilek P. Powering batteryless embedded platforms by piezoelectric transducers: A pilot study. *Elektron ir Elektrotechnika.* 2019 Apr; 25(2):32-5. <http://dx.doi.org/10.5755/j01.eie.25.2.23201>
12. Sheeraz MA, Butt Z, Khan AM, Mehmood S, Ali A, Azeem M, *et al.* Design and optimization of Piezoelectric Transducer (PZT-5H Stack). *J Electron Mater.* 2019 Oct; 48(10):6487-502. Available from: <https://doi.org/10.1007/s11664-019-07453-7>
13. Pradeesh EL, Udhayakumar S, Vasundhara MG, Kalavathi GK. A review on piezoelectric energy harvesting. Vol. 28, *Microsyst Technol.* 2022;28:1797-830. <https://doi.org/10.1007/s00542-022-05334-4>
14. Wang L, Zhao L, Jiang Z, Luo G, Yang P, Han X, *et al.* High accuracy comsol simulation method of bimorph cantilever for piezoelectric vibration energy harvesting. *AIP Adv.* 2019 Sep; 9(9) <https://doi.org/10.1063/1.5119328>

15. Chaudhuri D, Kundu S, Chatteraj N. Design and analysis of MEMS based piezoelectric energy harvester for machine monitoring application. *Microsyst Technol.* 2019 Apr; 25(4):1437-46. <https://doi.org/10.1007/s00542-018-4156-z>
16. Alsaadi N, Sheeraz MA. Design and optimization of bimorph energy harvester based on Taguchi and ANOVA approaches. *Alexandria Eng J.* 2020 Feb; 59(1):117–27. <https://doi.org/10.1016/j.aej.2019.12.016>
17. Mahapatra S Das, Mohapatra PC, Aria AI, Christie G, Mishra YK, Hofmann S, *et al.* Piezoelectric materials for energy harvesting and sensing applications: roadmap for future smart materials. *Adv Sci.* 2021; 8(17). <https://doi.org/10.1002/advs.202100864> PMID:34254467 PMCID:PMC8425885
18. Pradeesh EL, Udhayakumar S. Effect of placement of piezoelectric material and proof mass on the performance of piezoelectric energy harvester. *Mech Syst Signal Process.* 2019 Sep; 130:664-76. <https://doi.org/10.1016/j.ymssp.2019.05.044>